ACOUSTIC RESULTS FROM A FULL-SCALE WIND TUNNEL TEST EVALUATING INDIVIDUAL BLADE CONTROL

Stephen M. Swanson
Sterling Software, Inc.
Palo Alto, California

Stephen A. Jacklin
NASA Ames Research Center
Moffett Field, California

Achim Blaas
ZF Luftfahrttechnik, GmbH
Kassel-Calden, Germany

Georg Niesl
EUROCOPTER DEUTSCHLAND, GmbH
Munchen, Germany

Roland Kube
DLR, Institute of Flight Mechanics
Braunschweig, Germany

Abstract

A full-scale rotor was tested in the 40- by 80-Foot Wind Tunnel at NASA Ames Research Center's National Full-Scale Aerodynamics Complex to evaluate the effects of individual blade control (IBC) on rotor performance, vibrations and acoustics. Individual blade control was achieved by replacing the rotating pitchlinks with high-frequency hydraulic actuators. These actuators applied single harmonic inputs (2/rev to 6/rev) and multi-harmonic combinations (2/rev+4/rev, 3/rev+5/rev, etc.) at the blade root. The two acoustic conditions discussed in this paper are, a combination blade vortex interaction noise and rotor vibration condition, and a high blade vortex interaction noise condition. A microphone traverse system located below the advancing-side of the rotor was used to acquire advancing-side blade vortex interaction noise data. A 2/rev IBC input was found to generate large reductions in noise over the entire measurement area and a 2/rev+5/rev multi-harmonic combination generated a maximum 12 dB reduction at one microphone location with an average of 10 dB for the area measured. In addition to the reductions in blade vortex interaction noise, reductions in rotor vibrations were achieved for many of the inputs tested. The same 2/rev+5/rev combination input that generated noise reductions also significantly reduced the 4P rotor vibrations.

Presented at the American Helicopter Society 51st Annual Forum, Ft. Worth TX, May 9 - 11, 1995.

Notation

AMP_k	maximum amplitude of the individual blade control input, k = 2nd to 6th harmonic, deg
BL-SPL	band-limited sound pressure level, a metric of the overall acoustic energy in a range from 150 Hz to 1.5 kHz, (referenced to 20 μPa), dB
BVI	blade vortex interaction
c	speed of sound, ft/second
C_T	rotor thrust coefficient, $\text{Thrust}/[\pi R^2 \rho(\Omega R)^2]$
IBC	individual blade control
Mtip	hover tip mach number, ΩR/c
N	number of blades
nP	"n" cycles per rev, rotor harmonic
R	rotor radius, 16.1 ft
RTA	NASA/U.S. Army Rotor Test Apparatus
S	rotor reference area, ft^2
V	tunnel velocity, knots
α_s	shaft angle of attack, uncorrected for wind tunnel effects, positive nose up, deg

$\psi_{c,k}$ azimuth location of maximum positive peak for the cosine input function (0 deg with blade aft, increasing counter-clockwise looking down), k = 2nd to 6th harmonic, deg

μ rotor advance ratio, V/[ΩR]

$\theta_{c,k}$ amplitude of individual blade control input as a function of rotor azimuth, k = 2nd to 6th harmonic, deg

θ_n blade tip pitch derived from tip accelerometers as a function of rotor harmonic

ρ density of air, slugs/ft^3

σ rotor solidity, [N (chord)]/[πR]

Ω rotor rotational speed, rad/sec

ψ rotor azimuth angle (0 deg with blade aft, increasing counter-clockwise looking down), deg

Introduction

Rotorcraft continue to forge their place in society, utilizing their unique capabilities in a wide variety of ways. It is important, both in the military and in the civil sector, to minimize any negative impact rotorcraft have on the surrounding community. One area that has received increased attention is rotor acoustics. The reduction of noise generated by the rotor is necessary to maximize the utilization of rotorcraft while minimizing its impact on the surroundings.

In order to reduce or eliminate rotor noise, it is important to first understand the mechanisms behind it. A large amount of both theoretical and experimental data have been compiled to help understand the generation of rotor noise (Refs. 1 and 2). Two types of rotor noise have been identified as being the loudest and most annoying. These are high-speed impulsive (HSI) noise and blade vortex interaction (BVI) noise. HSI noise is generated in high-speed flight, when the local shock waves "delocalize" to the far field. Although this can be quite loud, it primarily occurs during high-speed flight conditions and tend to remain in-plane, not directed toward the ground. For flight in and around cities, BVI tends to be the more noticeable and annoying noise. Research has shown that BVI noise is generated during descent conditions, when the wake of the rotor is ingested and the blade tip vortices impinge on the blades.

Several methods have been evaluated for their ability to reduce BVI noise. Active controls have shown the most promise and have received a significant amount of attention. One method evaluated, and probably the most heavily documented, is higher-harmonic control (HHC) (Refs. 3 - 5). HHC applies high-frequency inputs to the rotor control system in the fixed frame, using high-frequency actuators to apply sinusoidal inputs to the swashplate. Although HHC has been shown to reduce BVI acoustics and rotor vibrations, these reductions have been limited due to placement of the system in the fixed frame. Due to design constraints of the swashplate, it is not possible for rotors with four or more blades to alter the pitch of one blade without changing the pitch of all blades simultaneously. Therefore, HHC inputs which allow the blades to follow similar pitch schedules (as a function of rotor azimuth) are limited to N-1 per rev, N per rev, and N+1 per rev, where N is the number of blades. To expand the number of harmonics that can be input, it is necessary to adjust the pitch of each blade individually. One method that had received recent attention has been the use of active blade flaps (Ref. 6). This system alters the pitch of each blade by deflecting small flaps located near the blade tip. While this has shown useful results, and does control each blade individually, this concept could be difficult to implement as it requires special rotor blades to be manufactured with, potentially, markedly different blade torsional stiffnesses.

A different method that has been evaluated varies the pitch of each blade via the blade root (IBC). As discussed in this paper, IBC has the capability to vary the blade pitch for any harmonic desired while ensuring that the pitch of all blades follows the same schedule around the rotor azimuth. This was implemented by replacing the rotating pitch links with hydraulic actuators.

A test of a full-scale BO 105 rotor system with IBC was conducted at the National Full-Scale Aerodynamics Complex (NFAC) 40- by 80-Foot Wind Tunnel. This was the second entry in an international program between NASA Ames Research Center, U.S. Army Aeroflightdynamics Directorate, ZF Luftfahrttechnik, EUROCOPTER DEUTSCHLAND and the DLR Institute for Flight Mechanics. The rotor system was tested on the NASA/U.S. Army Rotor Test Apparatus (RTA), modified with an IBC system. The primary objectives of this second entry were to evaluate the capability of IBC to suppress BVI noise, increase rotor performance, reduce rotor oscillatory loads, and alleviate rotor vibrations.

This report describes the test and highlights the effects of IBC on BVI noise and rotor vibration. A more complete discussion on the rotor vibration and performance results can be found in Ref. 7.

Test Description

The following section describes the tunnel, rotor and IBC hardware used in this test. The instrumentation, data

acquisition and analysis methods used in acquiring and reducing the acoustic and vibration data are also discussed. Additionally, a brief outline of the simulated flight conditions is given.

Hardware

The wind tunnel test was completed in the 40- by 80-Foot Wind Tunnel at NASA Ames Research Center's National Full-Scale Aerodynamics Complex. A conventional 4-bladed BO 105 rotor was mounted onto the NASA/U.S. Army Rotor Test Apparatus (RTA). Figure 1 shows the installation of the RTA, rotor and microphones in the test section. The RTA houses the drive motors, control systems and a steady/dynamic rotor balance. The balance measured the rotor hub loads and dynamic response of the system as it was effected by the IBC. A more detailed discussion on the wind tunnel, RTA and BO 105 rotor can be found in Refs. 8 - 10. Table 1 presents geometric data on the BO 105 rotor design.

Acoustic data were acquired with 7 microphones, 4 mounted below the advancing side of the rotor on a movable traverse system and 3 mounted below the retreating-side of the rotor on fixed stands. Figure 2 shows the general layout of the microphones with respect to the rotor. Table 2 lists the microphone locations relative to the rotor hub (for a rotor shaft angle of 0 deg) in Cartesian coordinates. The majority of acoustic data were acquired with the microphone traverse at one location for each test condition. For those IBC inputs that showed

Table 1:
General characteristics of the BO 105 rotor

Type	Hingeless
Radius (ft)	16.11
Number of blades	4
Blade chord (ft)	0.886
Linear blade twist (deg)	-8
Precone (deg)	-2.5
Solidity, σ	0.07
Reference area, S (ft^2)	57.1
Airfoil section	NACA 23012

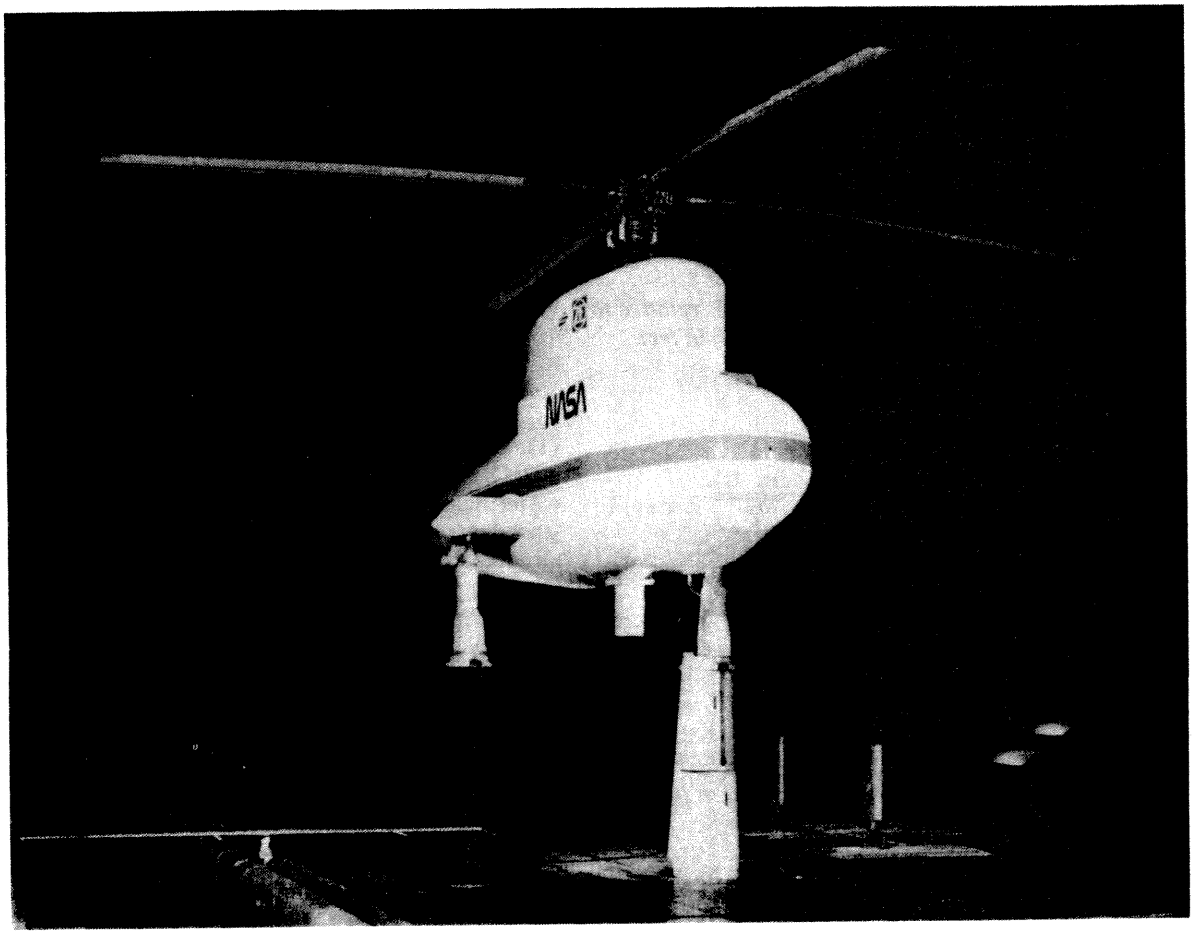

Figure 1. Installation of the RTA, rotor and microphones in the 40- by 80-Foot Wind Tunnel.

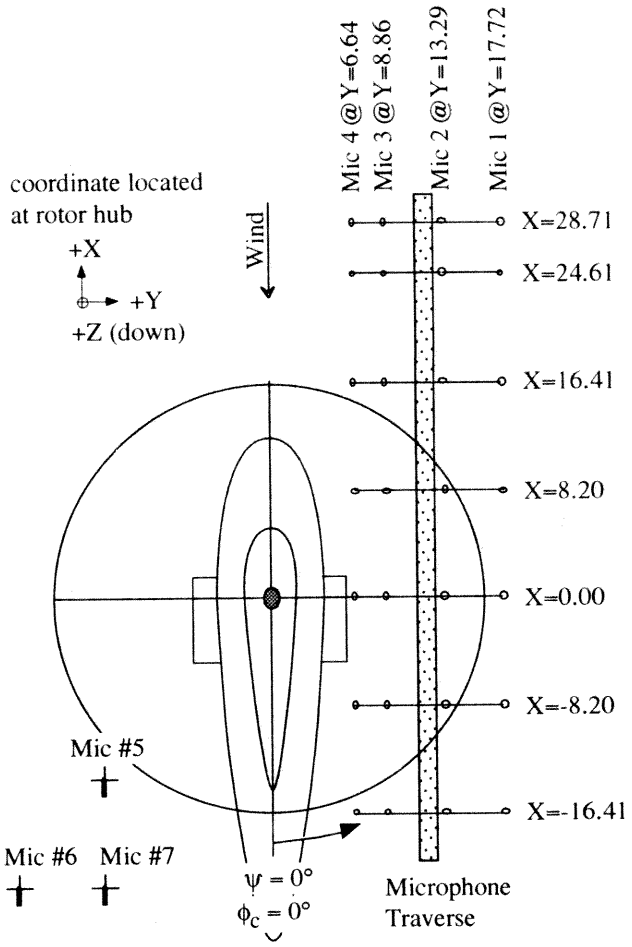

Figure 2. General layout of the microphones relative to the rotor and RTA, all dimensions in feet.

Table 2:
Microphone locations relative to rotor hub (distances in ft).

	X	Y	Z
Mic 1	*	17.72	18.86
Mic 2	*	13.29	18.86
Mic 3	*	8.86	18.86
Mic 4	*	6.64	18.86
Mic 5	-6.62	-13.29	14.12
Mic 6	-14.62	-13.29	14.12
Mic 7	-14.62	-8.86	14.12

* X location adjustable with the microphone traverse, X = -16.41, -8.20, 0.00, 8.20, 16.41, 24.61, 28.71.

substantial reductions in the acoustics, a sweep of the traverse was completed. These measurements were made in the near field, with the closest microphone location (0.00, 6.64) being 0.62 rotor diameters away from the hub and the farthest microphone location (28.71, 17.72) being 1.20 rotor diameters away.

Test Conditions

It is important to mention the method of rotor operation used during the test. The rotor and tunnel were brought to condition without the IBC system activated. The control positions were set for the desired hub pitch and roll moments, then a baseline data point was acquired. The IBC system was then activated. Since IBC was a control input, for most cases the trim state of the rotor altered. Trim was reset with the desired moments by adjusting the cyclic trim controls prior to acquiring data. This differed from the method used previously (Ref. 11), where flapping was minimized for all data points. Acoustic data were acquired for two test conditions. These are listed in Table 3 and are labeled as condition 1 and condition 2 throughout the paper. Some acoustic data were also acquired for condition 3, however this contained very little BVI noise and is not discussed. The principle microphone locations at which data were acquired with mic 3 at X=16.41 ft for condition 1 and with mic 3 at X=8.20 ft for condition 2.

Table 3:
Simulated Flight Conditions

	condition 1	condition 2	condition 3
	BVI and vibration	high-BVI	high-vibration
V (knots)	43	65	43
α_s	4.0	2.9	-2.4
Mtip	0.64	0.64	0.64
Mu	0.10	0.15	0.10
Ct/s	0.075	0.075	0.075
Hub roll moment	-300 ft-lbs	-350 ft-lbs	-300 ft-lbs
Hub pitch moment	1,400 ft-lbs	1,600 ft-lbs	1,400 ft-lbs

IBC System

The heart of the IBC system was the high-frequency actuators used to control each blade. Hydraulic actuators replaced each of the rotating pitch links of the conventional rotor control system. Designed by ZF Luftfahrttechnik, these actuators were capable of inputting sinusoidal pitch changes in the rotating frame over a range of 2P to 12P. Due to safety and hardware limitations, only the 2P through 6P inputs were tested. The maximum amplitude of IBC blade pitch was adjustable up to 3 deg for the 2P input, decreasing to 1.5 deg for the 6P input. Figure 3 is a schematic of an actuator installed on the rotor. Hydraulic pressure to power the actuators was delivered through a rotating hydraulic slipring located at the base of the rotor shaft.

Two redundant control computers, also designed by ZF Luftfahrttechnik, were used to command the actuators. The use of two separate computer systems minimized the

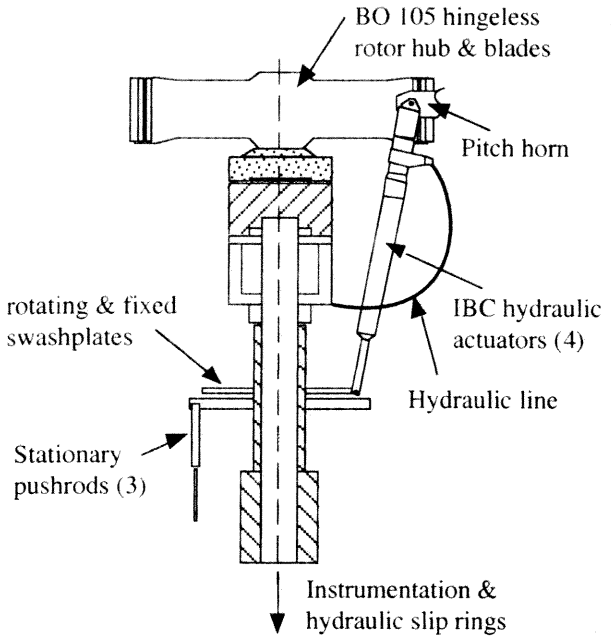

Figure 3. Cross section of rotor hub showing location of IBC actuator.

possibility of error due to uncontrolled actuator command. The system operator set the type of input desired (single-frequency or multi-frequency) and the phase of the input. The amplitude was then raised to the specified level.

Blade Motion

For this dynamic control system, the inputs were made at the blade root. Amplitude (AMP_k) describes the magnitude of the input sinusoidal function, while the phase ($\psi_{c,k}$) represents the location for the first positive peak of the cosine function. Equation 1 was used to describe the IBC blade root pitch as a function of the rotor

$$\theta_{c,k} = AMP_k * COS[P(\psi_i - \{i-1\}*[90\ deg] - \psi_{c,k})] \quad (1)$$

azimuth, phase input and amplitude. Note that the $\{i-1\} * [90\ deg]$ phase shift insures all four blades follow the identical high-frequency pitch schedule (where i is an integer representing each blade and k is the input harmonic). As presented in this paper, $\psi_{c,k}$ is the equivalent rotor azimuth location for the first positive peak of the cosine. Figure 4 shows an example of resultant blade root motion including both the conventional 1P input required for trimmed flight and the 2P IBC (AMP_k = 1.0 deg, $\psi_{c,2}$ = 50 deg). While this amplitude and phase information are adequate to describe the motion of the blade at the root, they do not adequately describe the motion of the blade tip. The blade dynamic characteristics will effect the pitch motion at the tip.

To gain an understanding of the effects of IBC on the blade tip motion, two accelerometers were mounted at the

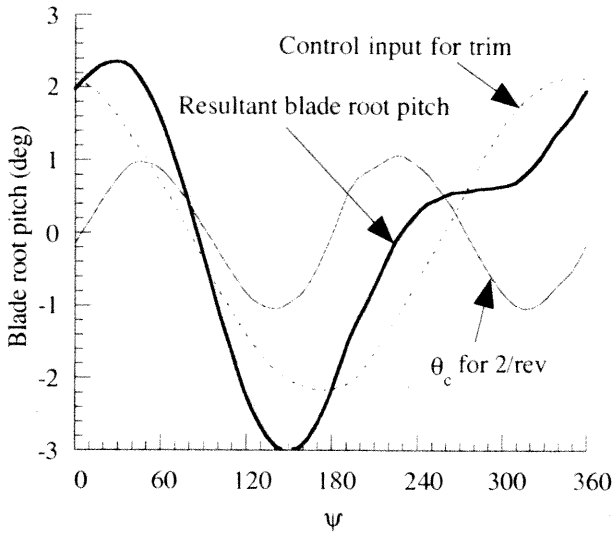

Figure 4. Example 2P single-frequency blade root input.

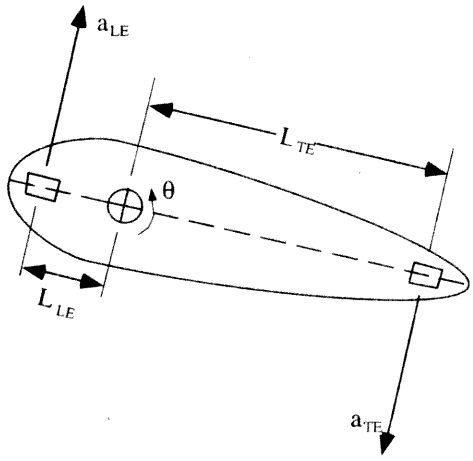

Figure 5. Schematic of blade tip accelerometers showing relative positions and sensing direction.

blade tip on the leading and trailing edges. A simplified relation between the accelerometer readings and the blade tip motion was derived. This is shown in Fig. 5 and expressed as Equation 2 (Ref. 10). Figure 6 shows the estimated blade tip motion for a 2P IBC input (condition

$$\theta_n = (a_{nLE} + a_{nTE}) / [\Omega^2(1-n^2)(L_{LE} + L_{TE})] \quad (2)$$

1, AMP_2 = 1.5 deg, $\psi_{c,2}$ = 30 deg). Note that Eqn. 2 does not account for any 1P motion (the $(1-n^2)$ would result in division by zero). While this simplified expression does not necessarily give the correct amplitude,

it does show the proper phasing of the higher harmonic blade tip pitch with respect to the rotor azimuth. This shows roughly a 10 deg phase lag of the blade tip to the input at the root for the 2P input. This phase lag increased with harmonic, up to 34 deg for the 6P input. Blade tip location information presented in this paper is, similar to the IBC input phase information, the azimuth location of the first positive peak of the cosine.

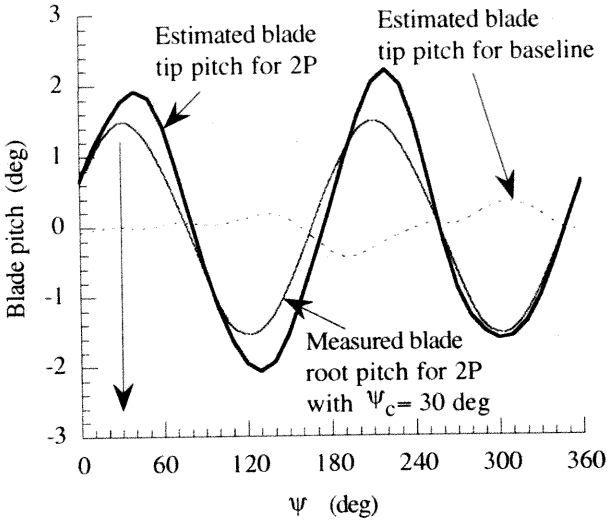

Figure 6. Derived blade tip motions for the baseline and a 2P IBC input; condition 1, 2P input with AMP_2 = 1.5 deg, Ψ_C = 30 deg.

Figure 6 shows not only the measured IBC actuator input at the blade root and the estimated blade tip motion for a 2P IBC input (from Eqn. 2), but it also shows the estimated blade tip pitch for the baseline (from Eqn. 2), no-IBC case. As expected, there is very little high-frequency blade pitch for the baseline case and a lack of 1P cyclic.

Data Acquisition and Analysis

Acoustic data were acquired using 7, 1/2 in condenser type microphones and stored on a digital tape deck. Data were recorded at a sample rate of 80 kHz, with a low-pass filter setting of 20 kHz. In addition, a 1/rev signal, 2048/rev signal and time code were also recorded for later use when analyzing the acoustic data.

To evaluate the data in a real-time manner, a signal from one microphone (usually the microphone at X=16.41, Y=8.86), was acquired on a dynamic signal analyzer. The analyzer generated an averaged time history (triggered off the 1/rev signal) and determined a power spectrum over 20 revolutions. The acoustic power level was then determined over a range from 150 Hz to 1500 Hz (approximately the 6th through 40th blade passage frequencies). This power level was used as an acoustic metric to evaluate, on a real-time basis, the effects of the IBC inputs being applied.

The data were analyzed in greater detail on a post-test basis, with averaged time histories and averaged frequency spectra over 40 rotor revolutions. Data were digitized from the tape recorder onto a personal computer at a rate of 2048 samples per revolution using an in-house program designed for acoustic reduction (Refs. 12 - 13).

FFT's were applied to the data over 8 revolutions, generating a bandwidth of 1.75 Hz per line, and averaged 5 times. From the resulting frequency spectrum, a metric was calculated to compare the effects of the IBC system on BVI noise. This band-limited sound pressure level (BL-SPL) metric was a summation of the frequency levels from 150 Hz to 1500 Hz (banding the 6th through 40th blade passage frequencies). This frequency range was found to contain the majority of the BVI energy and was chosen over standard dBA weighting because it highlights those frequencies which contain the majority of BVI energy (see Fig. 7). Due to the tunnel acoustic properties, below 500 Hz, the frequency spectra can become contaminated with low-frequency tunnel noise. A 150 Hz lower limit was chosen for the metric to include the dominant BVI energy. Above 1500 Hz, they become contaminated by the tunnel background noise. Reference 11 discusses this in more detail.

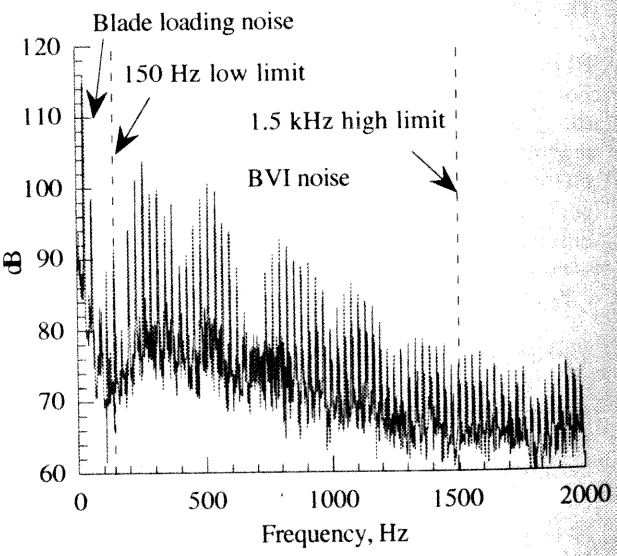

Figure 7. Baseline frequency spectrum showing the range of the BL-SPL metric: condition 1, microphone location (8.20, 8.86).

Vibration data were acquired using the RTA's steady/dynamic rotor balance, which measured up to the 20th harmonic of the rotor loads. To compare the vibration levels for different IBC inputs, the 4th harmonic component of the hub moment (a vector sum of the

pitching and rolling moments) as measured at the hub plane was determined. The 4P hub shear was also evaluated, but was found to closely follow the hub moments and is not presented. In this paper, vibration data are presented in conjunction with acoustic data, and are given in percent change from the baseline no-IBC values. More detailed information on the vibration metric and results from the test can be found in Ref. 7.

Results

Two types of IBC input were evaluated during this test program. The first used single-frequency inputs (2P to 6P) and the second used combinations of two or three different single-frequency inputs (2P + 3P or 2P + 3P + 5P, for example). Both types produced reductions and increases in the measured noise levels. Data for two different trim conditions are presented. Condition 1 was a combination BVI noise and rotor vibration condition, and condition 2 was a high-BVI noise condition.

Baseline BO 105 Data

Before discussing the effects of IBC, it is important to look at the baseline, no-IBC acoustic measurements. Figure 8 presents typical averaged time history data for condition 1 for a microphone located at a strong BVI location on the advancing-side of the rotor (high-pass filtered at 150 Hz to remove blade-loading noise). Time history data was non-dimensionalized (t/T) by dividing the time by the period for one revolution. This shows one strong BVI event for each rotor and several secondary events spread between each blade. These secondary events may be small interactions or they may be tunnel reflections. Although reflection tests were conducted to identify and minimize tunnel reflections, this was limited by tunnel and model mechanical requirements. The associated frequency spectrum was shown in Fig. 7, with a baseline BL-SPL value of 109.53 dB. For condition 2, the baseline value was 114.74 dB. Note that these BL-SPL values represent average values for different baseline data points acquired during the test. The overall uncertainty in the baseline levels for all conditions was ± 1.6 dB. This uncertainty is associated with slight differences when setting rotor trim and differences in tunnel static temperature.

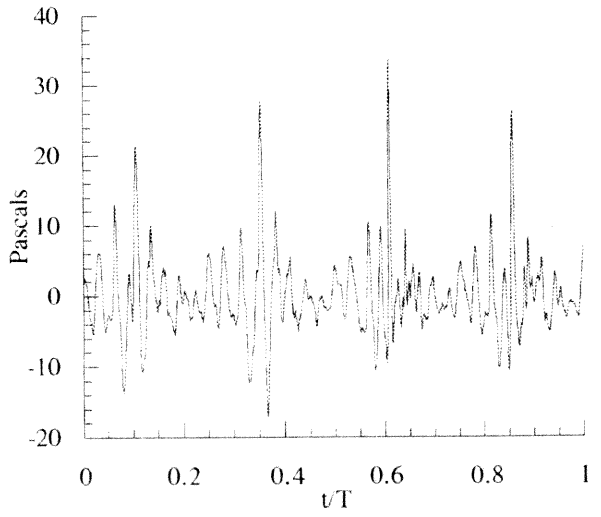

Figure 8. Averaged acoustic time history for a baseline (no IBC) condition; condition 1, microphone location (16.61, 8.86).

Figure 9 presents the BL-SPL values associated with a sweep of the microphone traverse system for the area shown in Fig. 2. The BL-SPL values displayed in this figure are not corrected for radial distance but are the levels measured at each of the microphone locations in the plane below the rotor. This shows the directivity of the BVI noise for condition 1. Averaged time history plots for one blade passage show several BVI events of similar amplitudes being measured below the advancing-side of the rotor (8.20, 6.64). Forward of the rotor (28.71, 8.86), a single BVI event becomes the dominant phenomena, and although the overall BL-SPL decreases, the peak-to-peak magnitude of the spike increases. A triangulation of this BVI event, using several different microphone locations, indicate the BVI occurred around the 60 deg azimuth range. Directly below and behind the rotor, the time histories contain a large number of secondary events. These could be either additional BVI events or tunnel reflections from the dominant events. Although the magnitude of these secondary events is small, they contain energy within the BL-SPL metric range and do contribute to the BL-SPL value.

Figure 10 shows the contour plot for condition 2 with no IBC inputs. Note the overall higher BL-SPL's for this condition as compared to Fig. 9. The directivity of the BL-SPL metric is in a more downward direction due to the two strong BVI events at (8.20, 6.64).

Single-Frequency Inputs

Figure 11 shows changes in the BL-SPL's for a 2P single-frequency input (condition 1, AMP_2 = 1.5 deg) with respect to the baseline levels for a sweep of phase angle. Reductions occurred for all phases, with maximums at $\psi_{c,2}$ = 30 deg and 135 deg (delta BL-SPL of -6.72 and -6.80 dB, respectively). From the blade tip accelerometers, the estimated blade tip peak locations were ψ = 40 and 140 deg azimuth. At first glance, these estimated blade tip pitch peaks would indicate IBC is effecting the BVI event (at ψ = 40 deg) and then the vortex generation (at ψ = 140 deg). However, since this is a 2P input, there are negative pitch peaks at $\psi_{c,2}$ + 90 deg and $\psi_{c,2}$ - 90 deg. Thus it is possible that IBC was effecting the vortex generation at ψ = 40 + 90 = 130 deg and then effecting the BVI event at ψ = 140 - 90 = 50 deg. Unfortunately, no information was available to pin-point

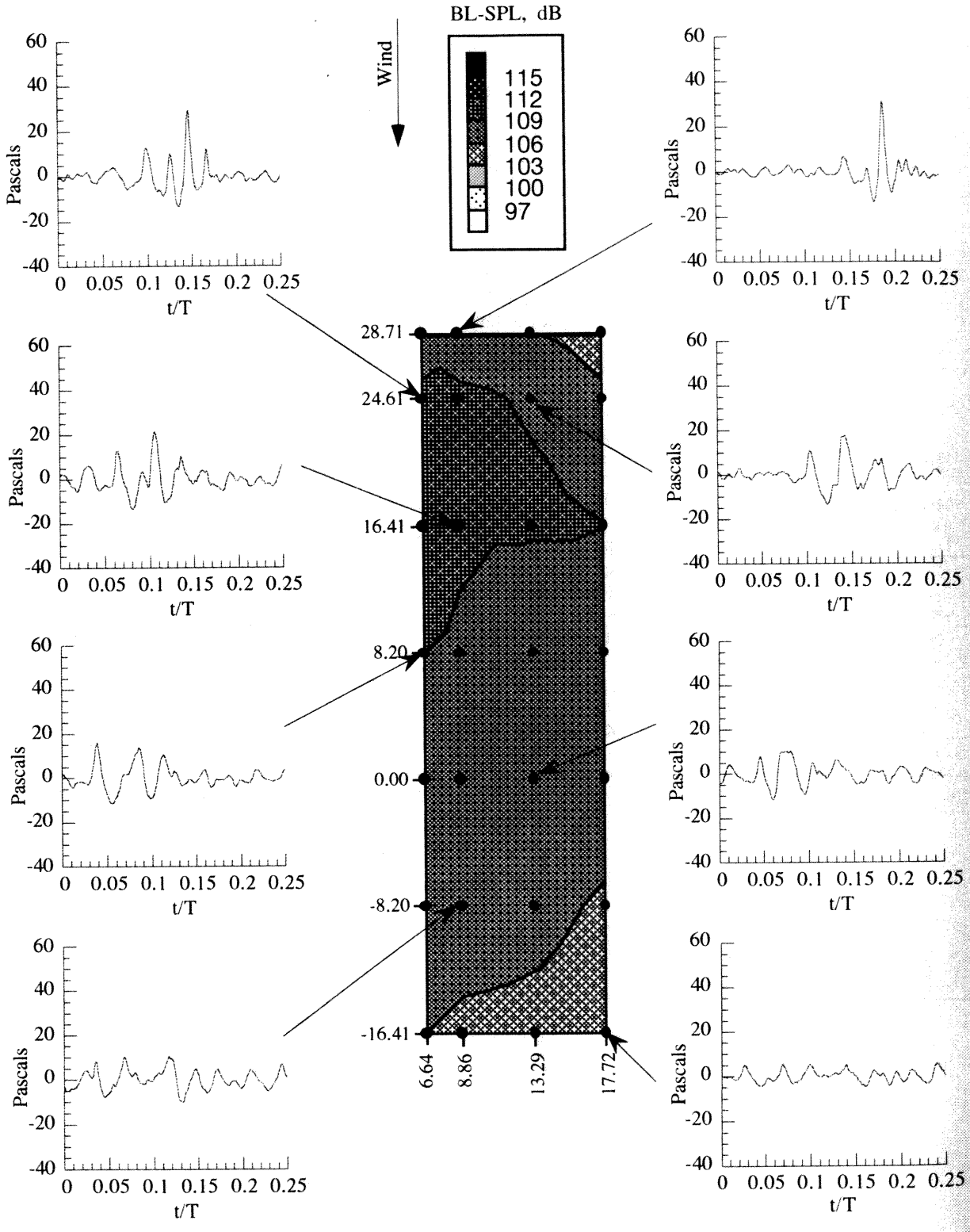

Figure 9. Contour plot of BL-SPL with averaged time histories for the baseline (no IBC) case; condition 1.

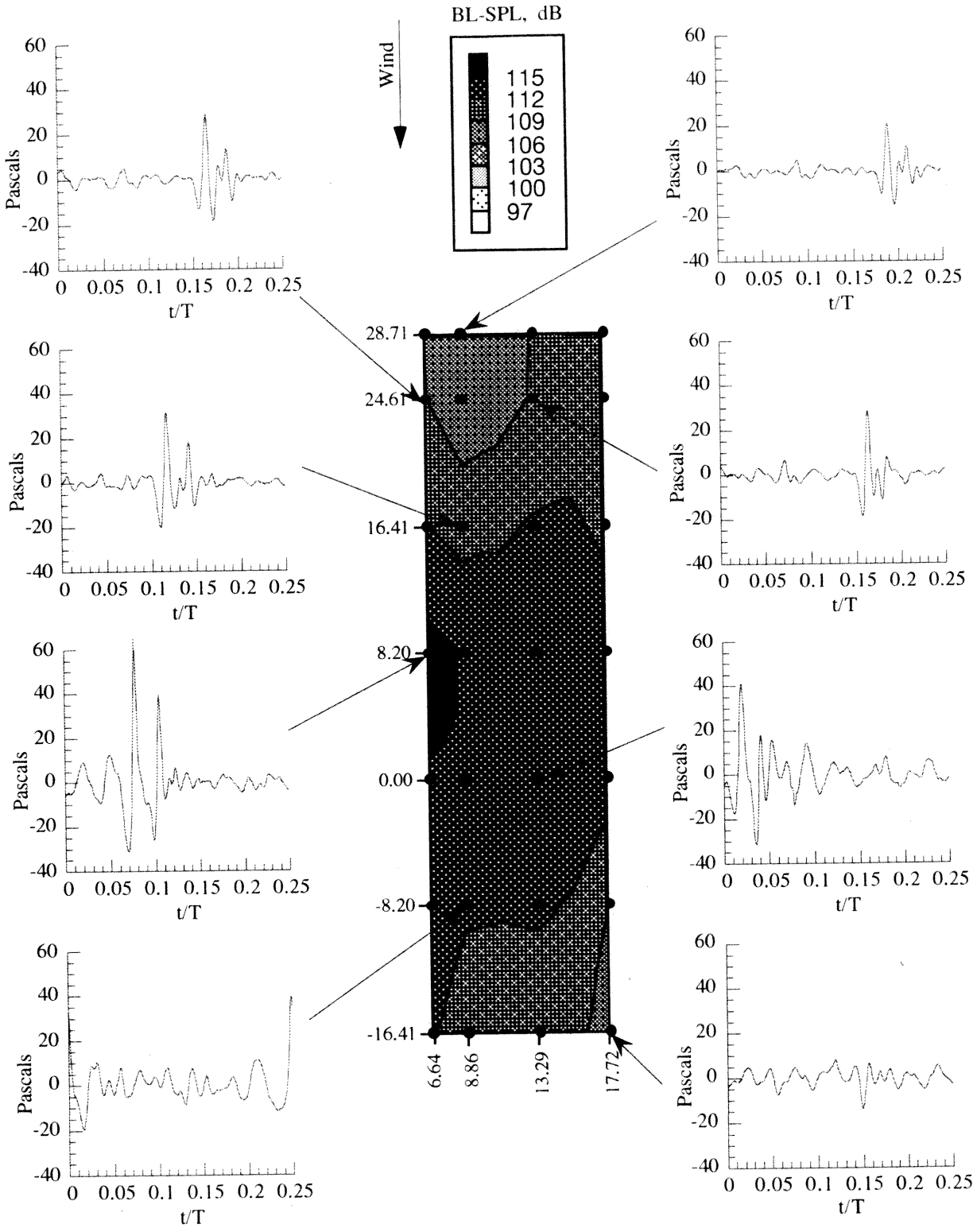

Figure 10. Contour plot of BL-SPL with averaged time histories for the baseline (no IBC) case; condition 2.

the location of the blade relative to the vortex. It is therefore difficult to determine whether the BVI event or the generation of the vortex is being effected by the IBC inputs.

The same 2P (AMP_2 = 1.5 deg) input effects are shown in Fig. 12 for condition 2 with changing phase angle. Note that reductions occur for the same inputs but with larger delta BL-SPLs (-9.5 and -6.6 dB, respectively).

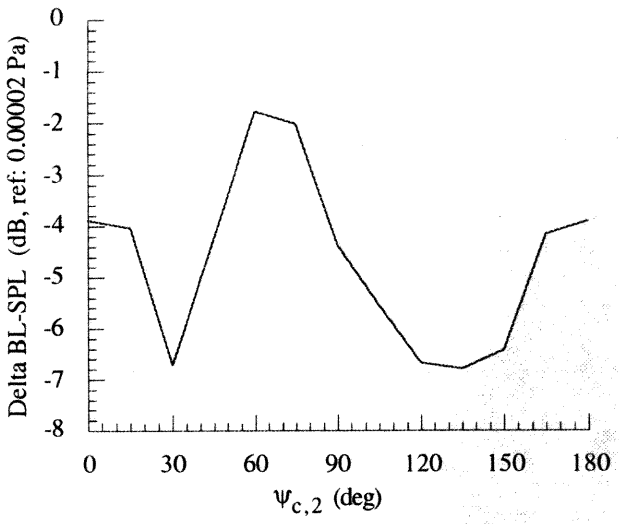

Figure 11. Variation in BL-SPL for a sweep of IBC phase with a 2P input; condition 1, microphone location (16.41, 8.86), AMP_2 = 1.5 deg.

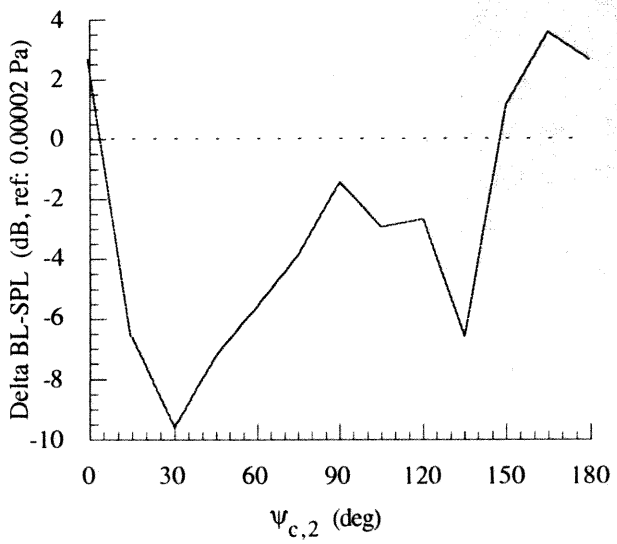

Figure 12. Variation in BL-SPL for a sweep of IBC phase with a 2P input; condition 2, microphone location (8.20, 8.86), AMP_2 = 1.5 deg.

To further understand the effects of the 2P IBC on the directivity of BVI, a sweep of the microphone traverse was made for those IBC inputs which best reduced the BL-SPL. Figure 13 shows a contour plot of the BL-SPL for the 2P IBC ($\psi_{c,2}$ = 30 deg, AMP_2 = 1.5 deg) input with several sample time histories. This can be compared to Fig. 9, the baseline, no-IBC condition. With IBC, an overall reduction in the BL-SPL values over the entire measurement area occurred. The sample time histories show a wide variety of effects on the BVI. A key result is the elimination of the primary BVI events forward of the rotor. The single, strong BVI previously associated with the 60 deg azimuth range is gone. Moving aft, the other large events were reduced substantially but not completely eliminated. For all of the time histories shown, the majority of the secondary events were reduced or eliminated. The shift in directivity aft is due to the reduction of the primary BVI events occurring the baseline case.

Figure 14 shows data for a sweep of the traverse with a 2P IBC input at condition 2 ($\psi_{c,2}$ = 30 deg, AMP_2 = 1.5 deg). Comparing with Fig. 10, dramatic reductions in the BL-SPL occurred at the forward locations (28.71, 8.86) and at locations below the rotor (8.20, 6.64). This was due primarily to the reduction of the BVI events forward and below the rotor. This caused the directivity of the BVI to shift in location toward the rear of the measurement area where little change is evident in the magnitude of the BVI (-8.20, 8.86). In this area the BL-SPL values remained consistent with the baseline case. Although the contour plots are not corrected for radial distances, the time history plots clearly show the IBC effects on the dominant BVI events.

Figures 15 and 16 show the BL-SPLs measured by the three retreating-side microphones for the 2P input (AMP_2 = 1.5 deg) at the two acoustic test conditions. For condition 1, reductions of up to 6 dB were measured at $\psi_{c,2}$ = 30 deg (Fig. 15). This matches well with the advancing-side reductions at the same input, however little retreating-side reductions occurred at $\psi_{c,2}$ = 135 deg. This is opposite for condition 2 (Fig. 16), where reductions of up to 8 dB were measured at $\psi_{c,2}$ = 90 and 110 deg, moderate reductions at 135 deg (4 dB), and increases at $\psi_{c,2}$ = 30 deg (2 to 4 dB). When discussing measurements acquired on the retreating-side, it is more appropriate to rotate the location of the cosine peaks. For the 2P input at $\psi_{c,2}$ = 30 deg, this would equate to 210 deg for the positive blade root pitch peak near vortex generation and 300 deg for the negative blade root pitch peak near the BVI event.

For condition 1, the effects of the 2P IBC (AMP_2 = 1.5 deg) on the 4P vibratory metric is shown in Fig. 17. The 4P hub moment experienced increases and decreases with respect to the different inputs, with a maximum reduction of 26.5 percent at $\psi_{c,2}$ = 15 deg. For the phase inputs

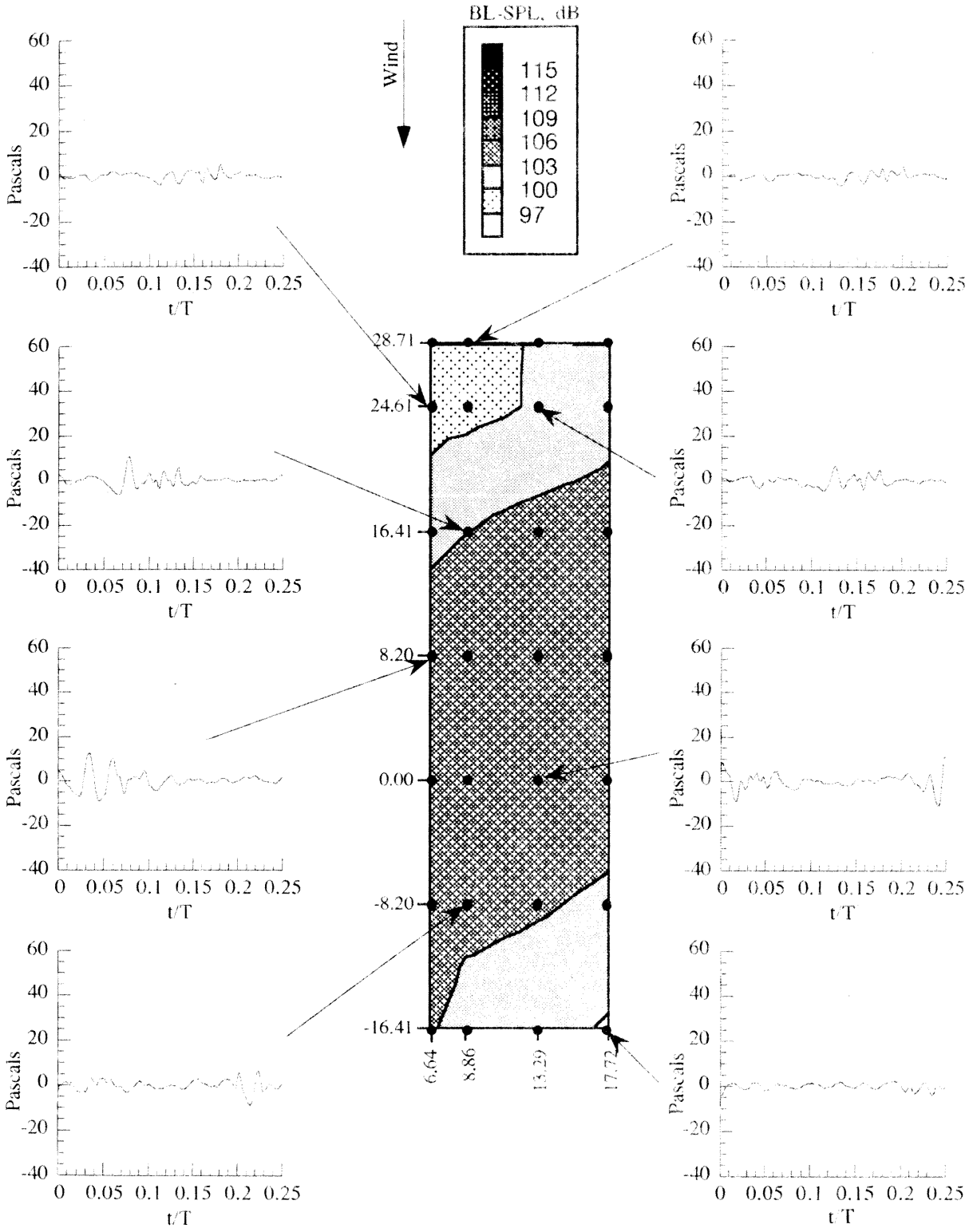

Figure 13. Contour plot of BL-SPL with averaged time histories for the 2P IBC case; condition 1, AMP_2 = 1.5 deg, $\psi_{C,2}$ = 30 deg.

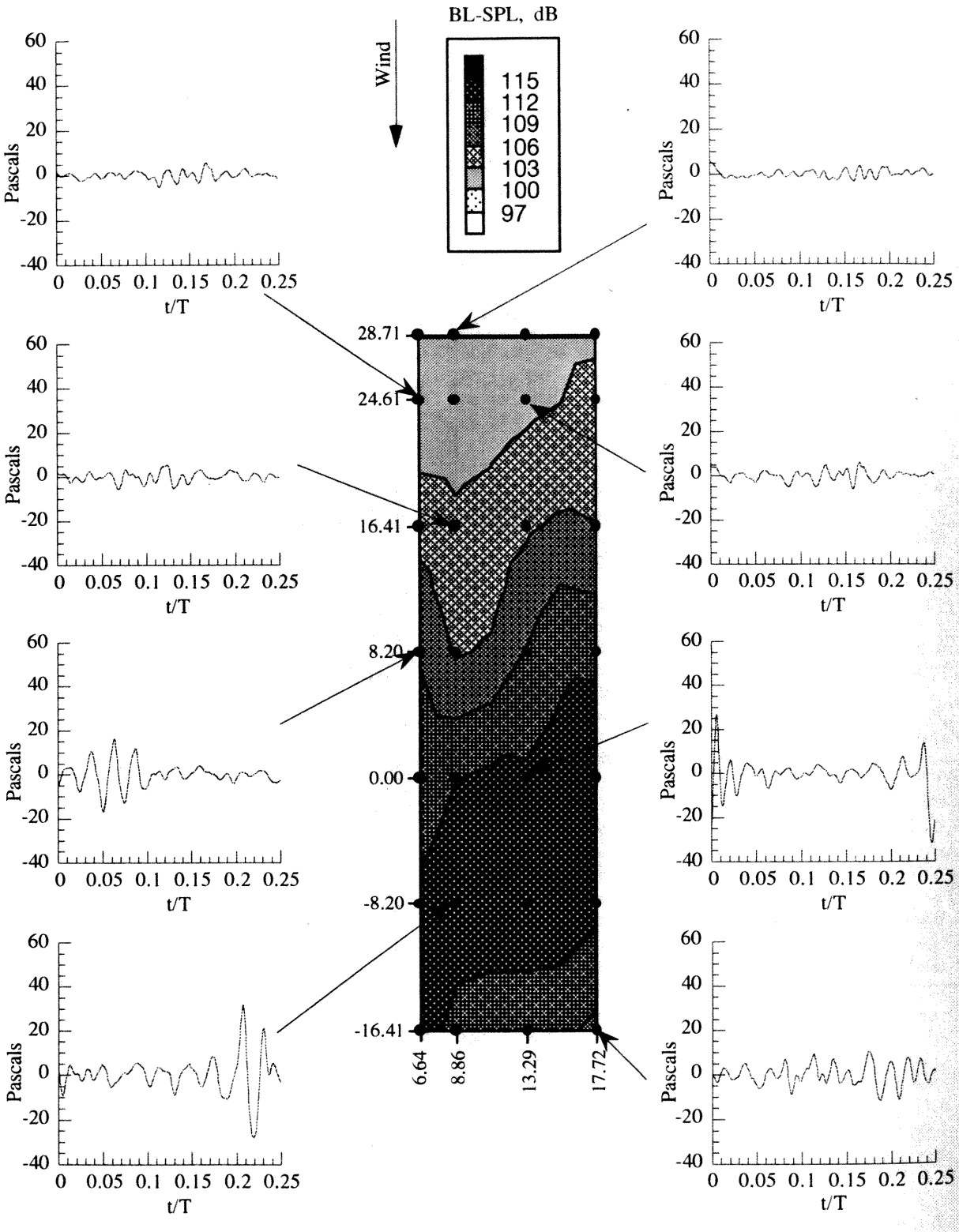

Figure 14. Contour plot of BL-SPL with averaged time histories for the 2P IBC case; condition 2, AMP_2 = 1.5 deg, $\psi_{c,2}$= 30 deg.

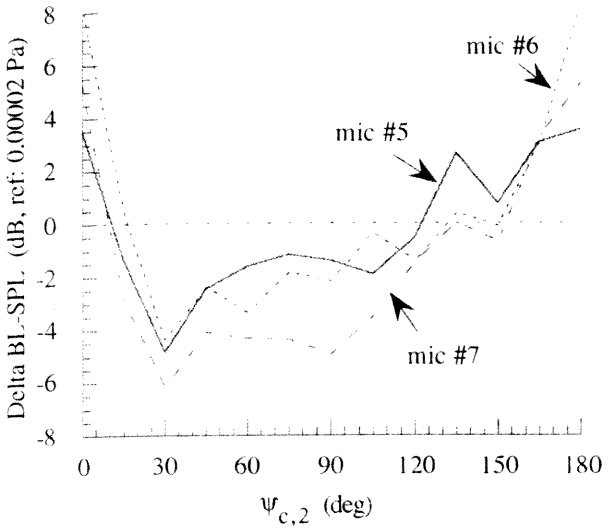

Figure 15. Variation in retreating-side BL-SPL for a sweep of IBC phase with a 2P input; condition 1, AMP_2 = 1.5 deg.

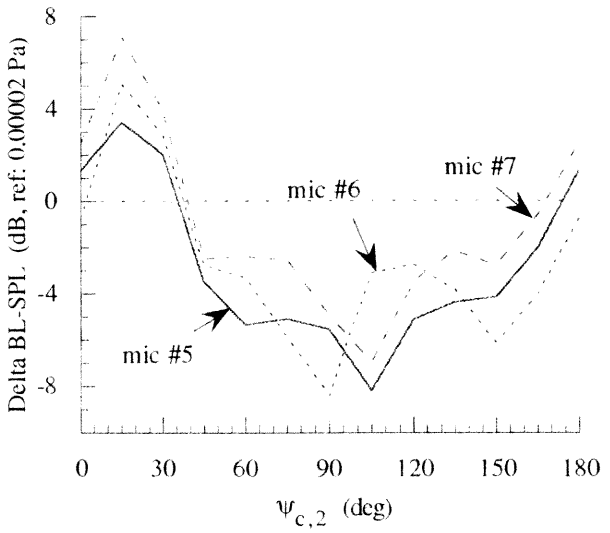

Figure 16. Variation in retreating-side BL-SPL for a sweep of IBC phase with a 2P input; condition 2, AMP_2 = 1.5 deg.

that generated the minimum acoustic BL-SPLs, reductions in the 4P hub moment occurred for one case (21 percent at $\psi_{c,2}$ = 30 deg), but increased dramatically at $\psi_{c,2}$ = 135 deg (146 percent).

Although somewhat useful for reducing acoustic levels, the 3P IBC input was not as effective as the 2P. A 3P single-frequency input was applied (AMP_3 = 1.0 deg), with acoustic results shown in Fig. 18 for condition 1. A general reduction in the BL-SPL for all input angles

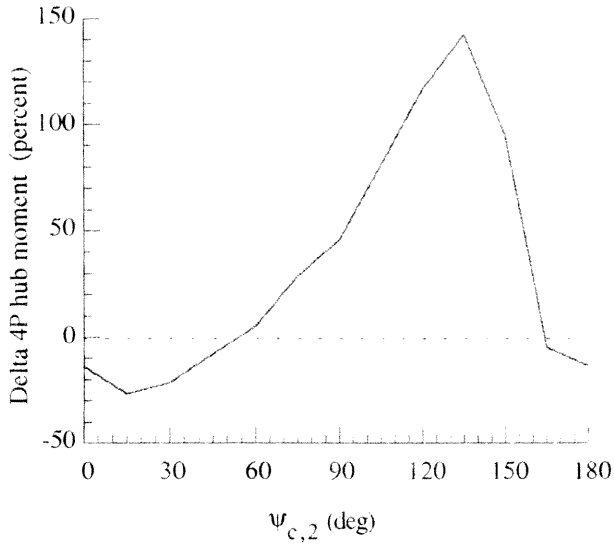

Figure 17. Effect of single 2P IBC input on 4P moments; condition 1, AMP_2 = 1.5 deg.

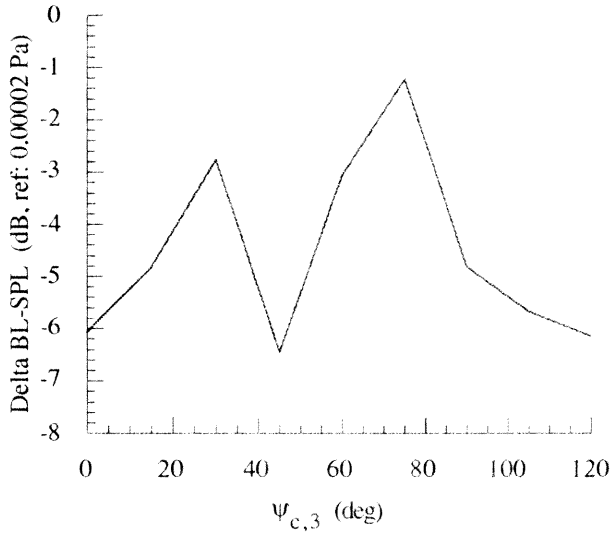

Figure 18. Variation in BL-SPL for a sweep of IBC phase with a 3P input; condition 1, microphone location (16.41, 8.86), AMP_3 = 1.0 deg.

occurred, with maximum reductions of 6.1 and 6.4 dB at $\psi_{c,3}$ = 0 deg and 45 deg, respectively. From the blade tip accelerometers, estimated locations of maximum blade tip pitch were 10 and 50 deg, respectively. Again it is difficult to determine the exact cause of the reduction since the cosine input repeats every 60 deg for the 3P input. For the $\psi_{c,3}$ = 0 deg, this puts a minimum blade root pitch peak at $\psi_{c,3}$ = 60 deg, near the BVI event, and a second blade root pitch peak at $\psi_{c,3}$ = 120 deg, near the vortex generation.

Figure 19 shows the retreating-side BL-SPLs for the 3P IBC (AMP_3 = 1.0 deg). This shows the same general trend for the three microphones with a maximum near $\psi_{c,3}$ = 60 deg, and minimums at 15 deg and near 90 to 105 deg.

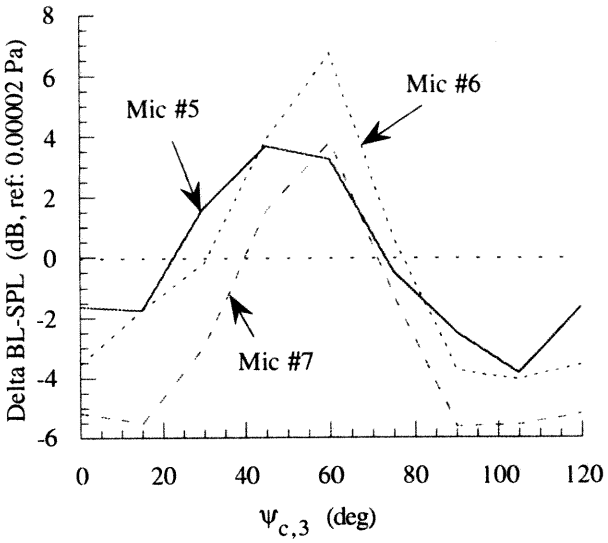

Figure 19. Variation in retreating-side BL-SPL for a sweep of IBC phase with a 3P input; condition 1, AMP_3 = 1.0 deg.

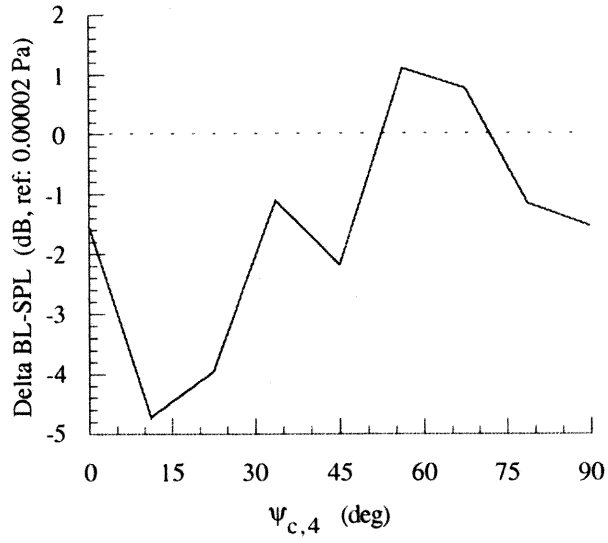

Figure 20. Variation in BL-SPL for a sweep of IBC phase with a 4P input; condition 1, microphone location (16.41, 8.86), AMP_4 = 0.5 deg.

Effects of a 4P IBC input (AMP_4 = 0.5 deg) on the BL-SPL are presented in Fig. 20 for condition 1. This shows a 4.7 dB reduction in the BL-SPL for $\psi_{c,4}$ = 11.25 deg with a second, smaller reduction at 45 deg. The estimated blade tip locations were 40 and 70 deg, respectively.

Figure 21 shows a sweep of the microphone traverse for the 4P IBC input (AMP_4 = 0.5 deg). The key difference between the 4P sweep and the baseline sweep (Fig. 9), is the reduction of the primary BVI event seen at the forward limit of the traverse (28.71, 8.86). This results in a shift of the directivity in the maximum BL-SPL to a location directly below the rotor where BVI still occur.

The corresponding vibration data for the 4P input (AMP_4 = 0.5 deg) is presented in Fig. 22. While this shows substantial reductions in the 4P hub moment at $\psi_{c,4}$ = 52.5 deg (50 percent), this does not correspond with the acoustic reductions. At this $\psi_{c,4}$, the BL-SPL increased (Fig. 20). For those $\psi_{c,4}$ that showed reductions in BL-SPL, the vibrations were increased above baseline.

For a 5P IBC single-frequency input (AMP_5 = 1.0 deg), an overall reduction in the BL-SPL metric is shown in Fig. 23, with a maximum reduction of 5.6 dB occurring at $\psi_{c,5}$ = 30 deg (condition 1 for microphone at (16.41, 8.86)). This had an estimated blade tip pitch peak of $\psi_{c,5}$ = 60 deg. The effect of the 5P IBC was not good on the 4P rotor vibration metric as it was on the acoustics. Figure 24 shows the variation in the 4P hub moments for a sweep of the 5P IBC input. For all phases the vibrations were increased anywhere from 100 to 200 percent.

The final single-frequency input tested was the 6P IBC (AMP_6 = 0.5 deg). The effect of the 6P IBC on the BL-SPL metric is shown in Fig. 24. The largest reductions in the BL-SPL (4.6 dB) occurred at $\psi_{c,6}$ = 50 deg. The estimated blade tip pitch peak was at 70 deg rotor azimuth. Reductions occurred only at one location due to the small range of azimuth available for the 6P input.

Multi-Frequency Inputs

To further explore the capabilities of the IBC system, multi-harmonic combinations were tested. These inputs were summations of the different single-frequencies, holding $\psi_{c,k}$ constant for one or more of the single-frequency inputs while varying the others. An example would be a 2P+3P input, where the 2P held a constant $\psi_{c,2}$ and the 3P $\psi_{c,3}$ varied from 0 to 120 deg. From the single-frequency inputs, the initial starting point was 2P IBC input at $\psi_{c,2}$ = 30 deg and AMP_2 = 1.5 deg with sweeps of $\psi_{c,k}$ for the 3P, 4P, 5P and 6P IBC.

Condition 1. Of these combination inputs, the best improvements in the BVI acoustic levels occurred with a

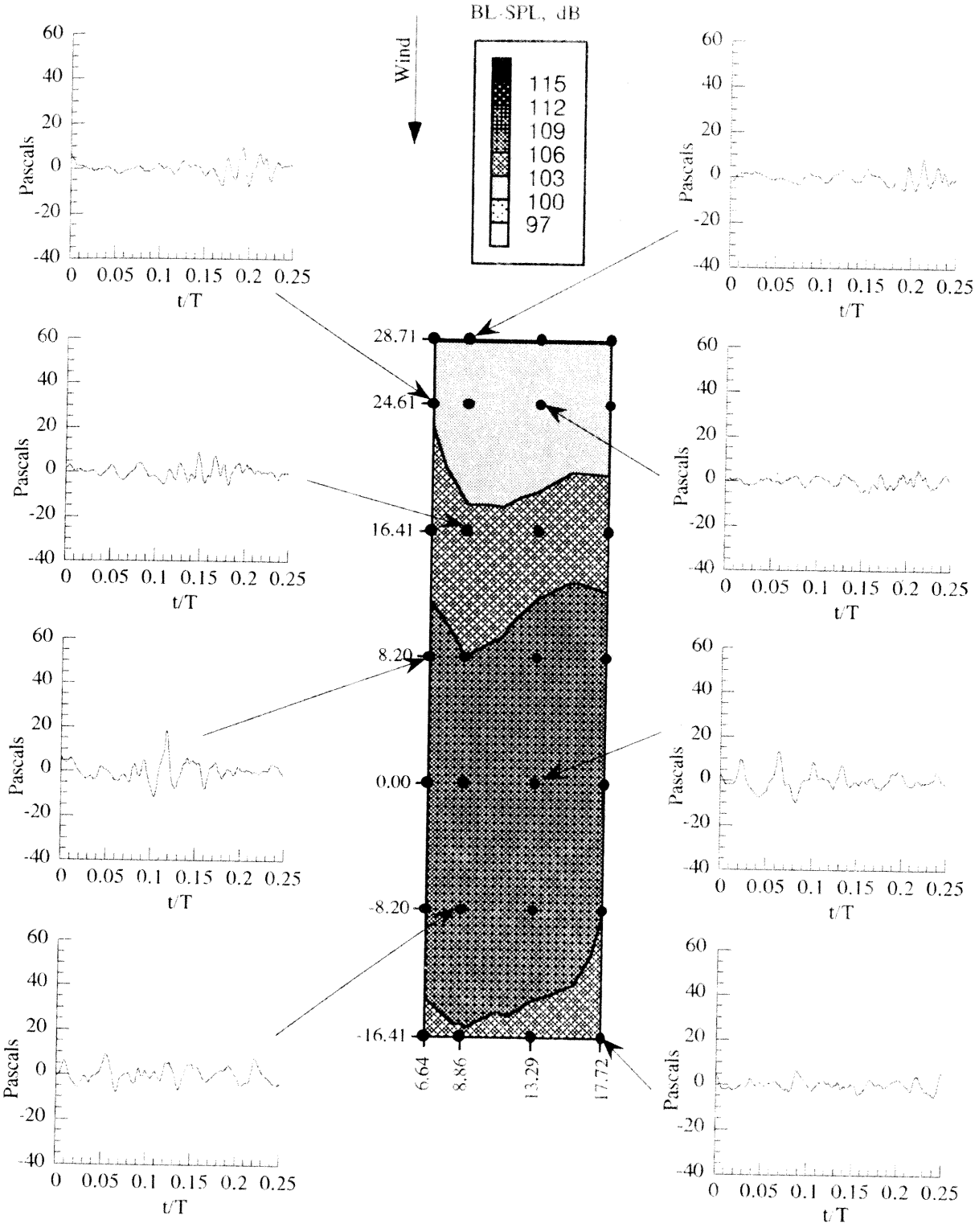

Figure 21. Contour plot of BL-SPL with averaged time histories for the 4P IBC case; condition 1, AMP_4 = 1.5 deg, $\psi_{c,4}$ = 30 deg.

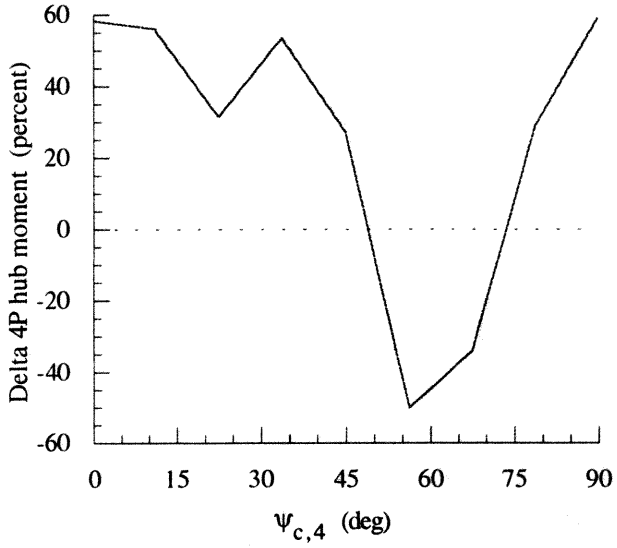

Figure 22. Effect of single 4P IBC input on 4P hub moments; condition 1, AMP_4 = 0.5 deg.

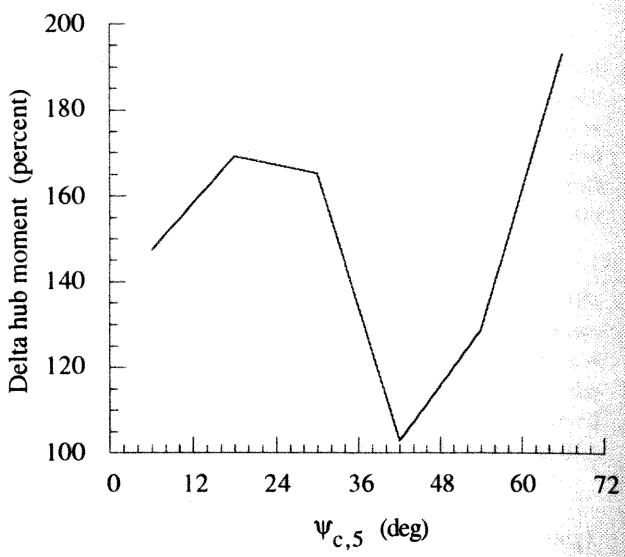

Figure 24 Effect of 5P IBC on the 4P hub moments; condition 1, AMP_5 = 1.0 deg.

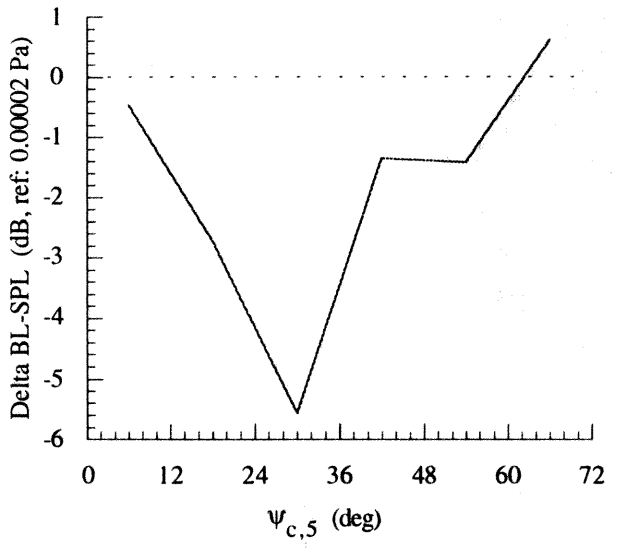

Figure 23. Variation in BL-SPL for a sweep of IBC phase with a 5P input; condition 1, microphone location (16.41, 8.86), AMP_5 = 1.0 deg.

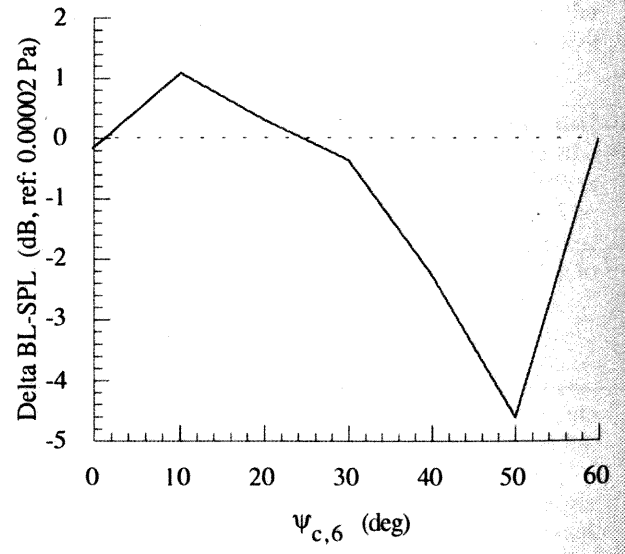

Figure 25. Variation in BL-SPL for a sweep of IBC phase with a 6P input; condition 1, microphone location (16.41, 8.86), AMP_6 = 0.5 deg.

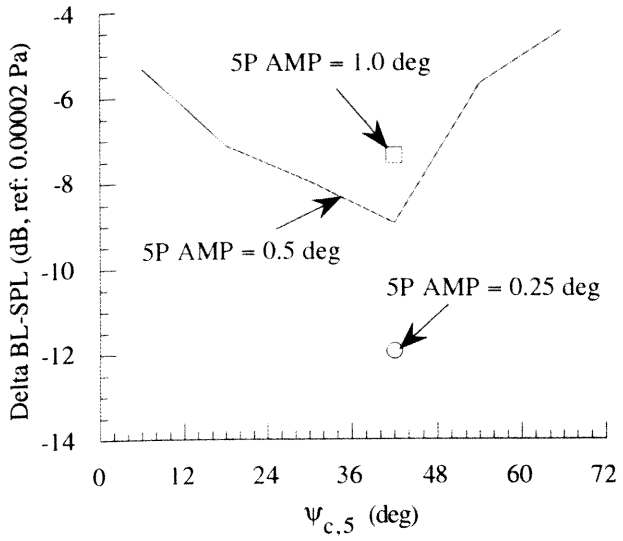

Figure 26. Effect of 2P+5P multi-harmonic IBC inputs on BL-SPL; condition 1, microphone location (16.41, 8.86), 2P with AMP_2 = 1.5 deg and $\psi_{c,2}$ = 30 deg.

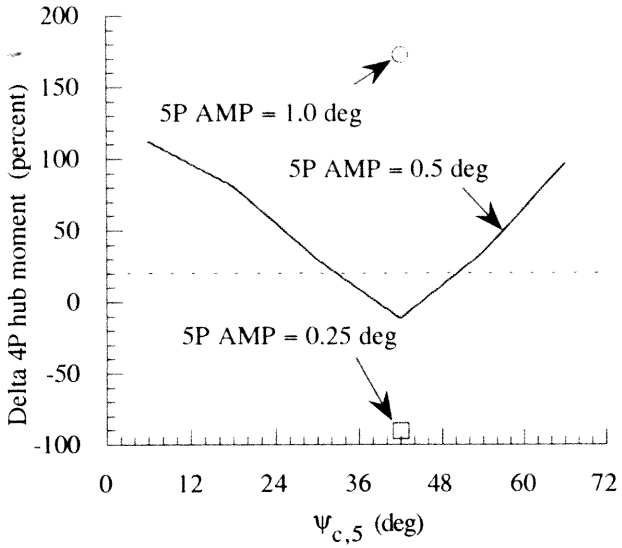

Figure 27. Effect of 2P+5P multiple harmonic IBC input on 4P hub moments; condition 1; 2P with AMP_2 = 1.5 deg and $\psi_{c,2}$ = 30 deg.

2P+5P input. The variation in the BL-SPL's for the 2P+5P IBC inputs is shown in Fig. 26. A reduction of 9 dB was measured when the 5P phase angle was 42 deg (AMP_5 = 0.5 deg, microphone location (16.41, 8.86)), roughly 2 dB lower then the levels reached with the 2P single-input. Further reduction in the BL-SPL were measured when a sweep of the 5P amplitude was completed. Figure 26 also shows a maximum reduction of 12 dB when the 5P amplitude was reduced to 0.25 deg while maintaining the 2P IBC with AMP_2 = 1.5 deg and $\psi_{c,2}$ = 30 deg.

Figure 27 presents the effects of the 2P+5P combination on the 4P vibration metric. This shows a reduction from baseline in the 4P moment at $\psi_{c,5}$ = 42 deg (5P AMP_5 = 0.5 deg) of 11 percent, and a 90 percent reduction when the 5P amplitude was reduced to 0.25 deg. Strong simultaneous reductions in the acoustics and vibrations occurred, improving on the single-frequency 2P input ($\psi_{c,2}$ = 30 deg). Increasing the 5P input to AMP_5 = 1.0 deg increased the rotor vibrations 170 percent over the baseline no-IBC conditions.

A sweep of the microphone traverse is presented in Fig. 28 with the 2P+5P combination for condition 1. The 2P input was held constant at $\psi_{c,2}$ = 30 deg, AMP_2 = 1.5 deg; and the 5P was held constant at $\psi_{c,5}$ = 42 deg, AMP_5 = 0.25 deg. This shows a reduction at all microphone locations where data were acquired. Of interest is the reduction of the major BVI events as seen with the 2P input, as well as a reduction in the secondary BVI events towards the rear of the rotor. Again, a shift in the location of maximum BL-SPL occurred, due to the elimination of the primary BVI events.

Measurements acquired by the retreating-side microphones for the 2P+5P input are presented in Fig. 29. This shows reductions for the sweep in 5P IBC (AMP_5 = 0.5 deg) at all $\psi_{c,5}$, with the trends for all microphones being similar. From Fig. 16, for the 2P IBC with 1.5 deg

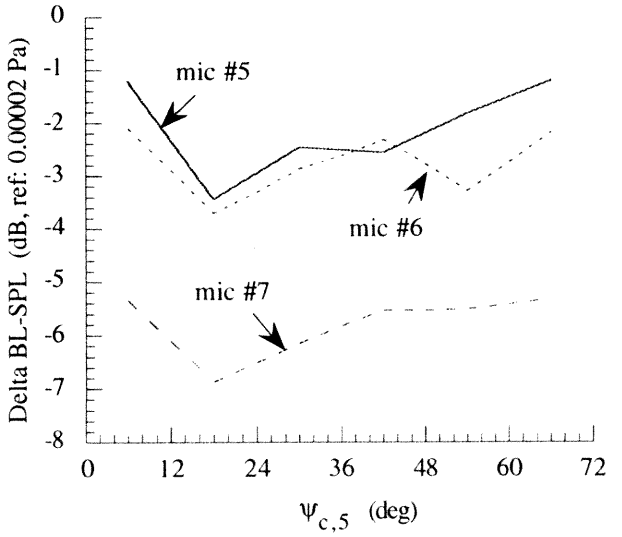

Figure 29. Variation in retreating-side BL-SPL for a sweep of IBC phase with 2P+5P input; condition 1, 2P with AMP_2 = 1.0 deg and $\psi_{c,2}$ = 30 deg, 5P AMP_5 = 0.5 deg.

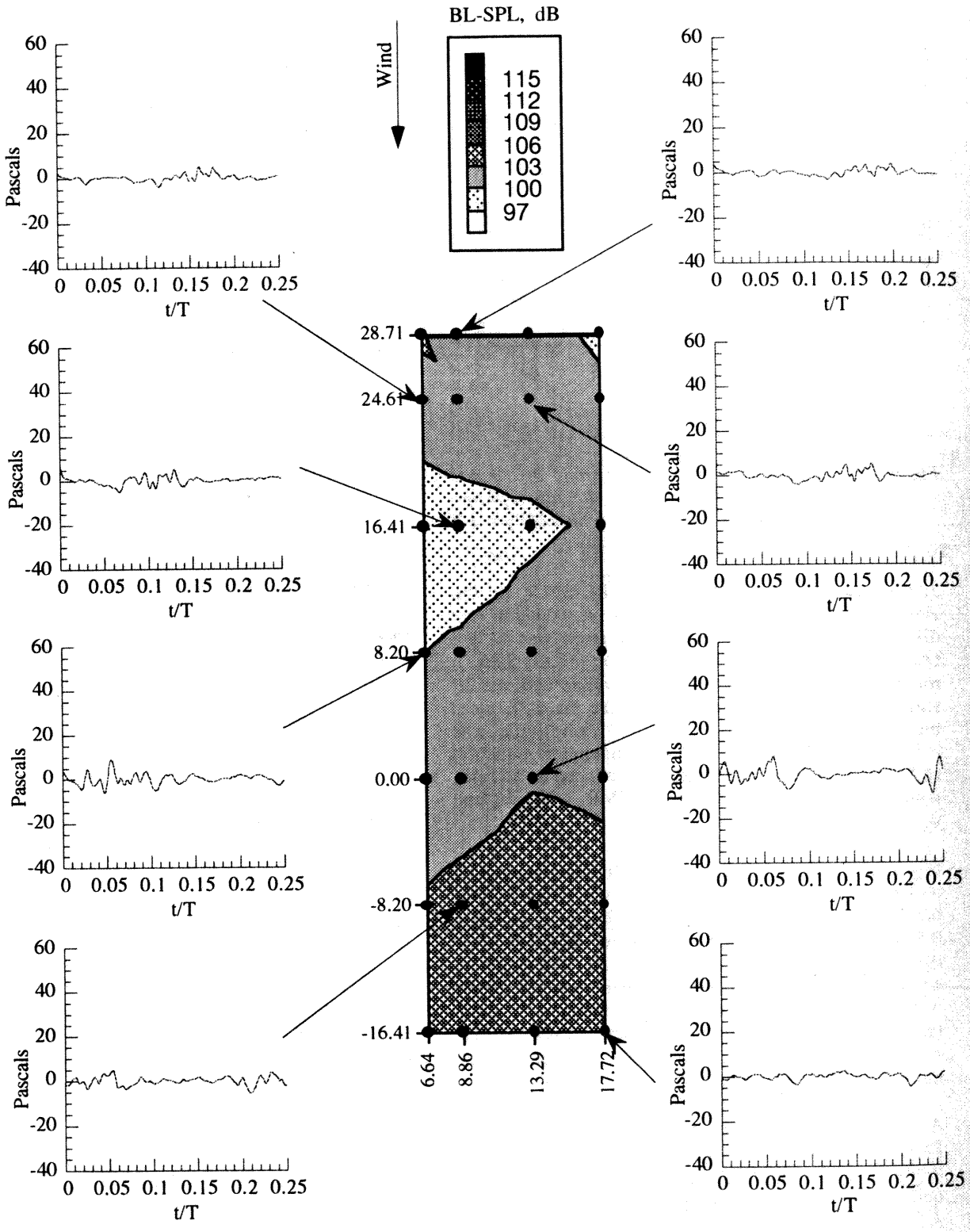

Figure 28. Contour plot of BL-SPL with averaged time histories for the 2P - 5P IBC case; condition 1, 2P with AMP_2 = 1.5 deg, $\psi_{c,2}$ = 30 deg, 5P with AMP_5 = 0.25 deg, $\psi_{c,5}$ = 42 deg.

AMP_2 at $\psi_{c,2}$ = 30 deg, there were slight increases in the retreating side noise. Any increases that did occur with the 2P+5P combination were due to the addition of the 5P input on top of the 2P input. The best reductions occurred for all microphones at $\psi_{c,5}$ = 18 deg.

Condition 2. Figure 30 shows a similar phase angle sweep of the 5P with AMP_5 = 0.5 deg for the 2P+5P combination, but for trim condition 2. Reductions in the BL-SPL for the microphone location examined (8.20, 8.86) were a maximum of 9.2 dB for the 2P+5P. This was similar in magnitude to the results found for the 2P single-frequency input.

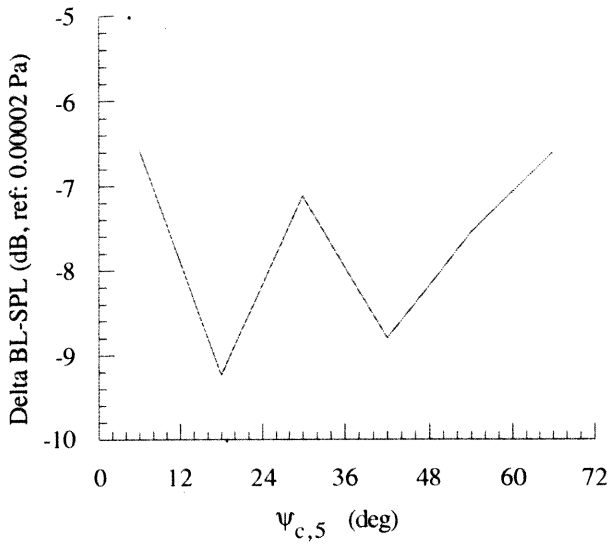

Figure 30. Effect of 2P+5P multi-harmonic IBC inputs on BL-SPL; condition 2, microphone location (8.20, 8.86), 2P with AMP_2 = 1.0 deg and $\psi_{c,2}$ = 30 deg, 5P AMP_5 = 0.5 deg.

Conclusions

A joint international wind tunnel test was conducted at NASA Ames Research Center to evaluate the effect of individual blade control on blade vortex interaction noise and on rotor vibrations.

The following conclusions were drawn:

Single-frequency IBC inputs,

1. Reductions in the acoustic BVI noise levels were achieved for all single-frequency inputs. For the data presented at one microphone location at a mixed BVI noise and rotor vibration trim condition, reductions for all single-frequency inputs (2P, 3P, 4P, 5P, and 6P) were on the order of 5 dB. A maximum 6.7 dB reduction was measured with the 2P IBC input.

2. With 1.5 deg of 2P IBC single-frequency input, a maximum reduction of 9.8 dB was achieved for a high-BVI noise flight condition at one microphone location.

3. Simultaneous reductions in acoustics and vibrations were achieved with a 2P single-frequency input. A 21 percent reduction in the rotor 4P hub moment was achieved simultaneously with the 6.7 dB reduction in the advancing-side BVI noise.

Multi-frequency IBC inputs,

4. A combination input of 2P+5P IBC achieved the best reductions in BVI noise. A 12 dB reduction was measured at one microphone location for the mixed BVI noise and rotor vibration trim condition. For the high-BVI noise condition, reductions of 8.8 dB were measured.

5. The 2P+5P combination also gave better vibration reductions over the single-frequency 2P input. A maximum 90 percent reduction in rotor 4P vibrations were measured below the baseline no-IBC condition.

General,

6. Through the use of an acoustic traverse, the effect of different IBC inputs on advancing-side noise directivity was evaluated. Any changes in the directivity were attributed to reductions in primary BVI events.

7. All of the inputs showed positive and negative effects on the BVI acoustics. And while the causes of BVI noise are known, no information was available as to the relative blade and vortex interaction spacing or the vortex strength. It was therefore difficult to determine the exact reasons for the reductions in BVI noise.

Acknowledgments

The authors wish to thank Ms. Melani Reddy for her dedicated help in reducing the acoustic data acquired during this test.

References

1. Schmitz, F. H., Boxwell, D. A., Lewy, S. and Dahan, C., "Model- to Full-Scale Comparisons of Helicopter Blade-Vortex Interaction Noise," American Helicopter Society 38th Annual Forum, Anaheim, CA, May 1982.

2. Schmitz, F. H., Boxwell, D. A. and Vause, C. R., "High-Speed Helicopter Impulsive Noise," *Journal of the American Helicopter Society*, Vol. 22, No. 4, Oct. 1977.

3. Splettstoesser, W. R., Lehmann, G. and Van Der Wall, B., "Initial Results of a Model Rotor Higher Harmonic Control (HHC) Wind Tunnel Experiment of BVI Impulsive Noise Reduction," Fifteenth European

Rotorcraft Forum, Amsterdam, The Netherlands, Sept. 1989.

4. Splettstoesser, W. R., Schultz, K.-J., Kube, R., Brooks, T. F., Booth Jr., E. R., Niesl, G. and Streby, O., "BVI Impulsive Noise Reduction by Higher Harmonic Pitch Control: Results of a Scaled Model Rotor Experiment in the DNW," Seventeenth European Rotorcraft Forum, Berlin, Germany, Sept. 1991.

5. Kottapalli, S., Swanson, S., LeMasurier, P. and Wang, J., "Full-Scale Higher Harmonic Control Research to Reduce Hub Loads and Noise," American Helicopter Society 49th Annual Forum, St. Louis, MO, May 1993.

6. Marcolini, M. A., Booth Jr., E. R., Tadghighi, H., Hassan, A., Smith, C. and Becker, L. E., "Control of BVI Noise Using an Active Trailing Edge Flap," American Helicopter Society Vertical Lift Conference, San Francisco, CA, Jan. 1995.

7. Jacklin, S. A., Blaas, A., Teves, D. and Kube, R., "Reduction of Helicopter BVI Noise, Vibration, and Power Consumption Through Individual Blade Control," American Helicopter Society 51st Annual Forum, Fort Worth, TX, May 1995.

8. Norman, T. R., Cooper, C. R., Fredrickson, C. A. and Herter, J. R., "Full-Scale Wind Tunnel Evaluation of the Sikorsky Five-Bladed Bearingless Main Rotor," American Helicopter Society Aeromechanics Specialists Conference, San Francisco, CA, Jan. 1994.

9. Shinoda, R. and Johnson, W., "Performance Results from a Test of an S-76 Rotor in the NASA Ames 80- by 120-Foot Wind Tunnel," AIAA Applied Aerodynamics Conference, Monterey, CA, Aug. 1993.

10. Jacklin, S. A., Nguyen, K. Q., Blaas, A. and Richter, P., "Full-Scale Wind Tunnel Test of a Helicopter Individual Blade Control System," American Helicopter Society 50th Annual Forum, Washington, D.C., May 1994.

11. Swanson, S. M., Jacklin, S., A., Blaas, A., Kube, R. and Neisl, G., "Individual Blade Control Effects on Blade-Vortex Interaction Noise," American Helicopter Society 50th Annual Forum, Washington D. C., May 1994.

12. Watts, M. E., "ALDAS User's Manual." NASA TM 102381, April 1991.

13. Watts, M.E. and St. Jean, M. M., "Data Acquisition and Analysis on a Macintosh," American Helicopter Society International Specialist Meeting on Rotorcraft Acoustics and Rotor Dynamics, Philadelphia, PA, Oct. 1991.